

Thermal conduction in a mirror-unstable plasma

S. V. Komarov^{1,2*}, E. M. Churazov^{1,2}, M. W. Kunz³ and A. A. Schekochihin^{4,5}

¹*Max Planck Institute for Astrophysics, Karl-Schwarzschild-Strasse 1, 85741 Garching, Germany*

²*Space Research Institute (IKI), Profsovnaya 84/32, Moscow 117997, Russia*

³*Department of Astrophysical Sciences, Princeton University, Princeton, NJ 08544, United States*

⁴*The Rudolf Peierls Centre for Theoretical Physics, University of Oxford, 1 Keble Road, Oxford OX1 3NP, United Kingdom*

⁵*Merton College, Oxford OX1 4JD, United Kingdom*

9 October 2018

ABSTRACT

The ICM plasma is subject to firehose and mirror instabilities at scales of order the ion Larmor radius. The mirror instability generates fluctuations of magnetic-field strength $\delta B/B \sim 1$. These fluctuations act as magnetic traps for the heat-conducting electrons, suppressing their transport. We calculate the effective parallel thermal conductivity in the ICM in the presence of the mirror fluctuations for different stages of the evolution of the instability. The mirror fluctuations are limited in amplitude by the maximum and minimum values of the field strength, with no large deviations from the mean value. This key property leads to a finite suppression of thermal conduction at large scales. We find suppression down to ≈ 0.2 of the Spitzer value for the secular phase of the perturbations' growth, and ≈ 0.3 for their saturated phase. The effect operates in addition to other suppression mechanisms and independently of them. Globally, fluctuations $\delta B/B \sim 1$ can be present on much larger scales, of the order of the scale of turbulent motions. However, we do not expect large suppression of thermal conduction by these, because their scale is considerably larger than the collisional mean free path of the ICM electrons. The obtained suppression of thermal conduction by a factor of ~ 5 appears to be characteristic and potentially universal for a weakly collisional mirror-unstable plasma.

Key words: plasmas, conduction, magnetic fields, instabilities

1 INTRODUCTION

Thermal conduction in a magnetized plasma is a long-standing problem in astrophysics, dating back to the realization that virtually all astrophysical plasmas possess magnetic fields (based on both theoretical considerations and observations of synchrotron emission and the Faraday rotation). Although these fields are relatively weak ($\sim 1\text{--}10\ \mu\text{G}$ in the bulk of the ICM, see, e.g., Carilli & Taylor 2002 or Feretti et al. 2012 for reviews), they constrain the motion of charged particles to spiraling along the field lines with Larmor radii typically very small compared to other physically relevant scales, namely, to the collisional mean free path and the correlation length of the plasma flows. In such a plasma, the electrons predominantly transfer heat along the field lines.

In the ICM, the quest for a theory of effective heat conductivity is strongly motivated by the observations of apparently long-lived temperature substructures (e.g., Markevitch et al. 2003) and sharp gradients (cold

fronts, e.g., Markevitch et al. 2000; Ettori & Fabian 2000; Vikhlinin et al. 2001; Markevitch & Vikhlinin 2007) that would not have survived had the electron conductivity been determined by the classic Spitzer expression for an unmagnetized plasma (Spitzer 1962). Another puzzling topic is the stability of cluster cool cores, in which the role of thermal conduction is still unclear (e.g., Ruszkowski & Begelman 2002; Zakamska & Narayan 2003; Voigt & Fabian 2004; Dennis & Chandran 2005).

The general problem of thermal conduction in an astrophysical plasma is greatly complicated by the fact that the medium is likely turbulent (for the ICM, see, e.g., Inogamov & Sunyaev 2003; Schuecker et al. 2004; Schekochihin & Cowley 2006; Subramanian et al. 2006; Zhuravleva et al. 2014), and so the magnetic-field lines are randomly tangled. It is practical to subdivide the problem into more narrowly formulated questions and study them separately. First, parallel conduction in a static magnetic field of a given structure can be investigated (e.g., Chandran & Cowley 1998). The static approximation is reasonable because electrons stream along magnetic fields faster than these fields are evolved by turbulence. Next,

* E-mail: komarov@mpa-garching.mpg.de

one can study the effective boost of the transverse conduction across the field lines due to their exponential divergence (Skilling et al. 1974; Rechester & Rosenbluth 1978; Chandran & Cowley 1998; Narayan & Medvedev 2001; Malyshkin 2001; Chandran & Maron 2004). Finally, local heat fluxes at the scale of turbulent eddies are affected by the correlation between temperature gradients and the magnetic field as they evolve in the same turbulent velocity field (Komarov et al. 2014; this process occurs on longer time scales than the other two). In this work, we only address the first part of the problem, parallel thermal conduction, as applied to the ICM.

Parallel conduction can be affected by magnetic trapping of electrons by fluctuations of the field strength along a field line (Klepach & Ptuskin 1995; Chandran & Cowley 1998; Chandran et al. 1999; Malyshkin & Kulsrud 2001; Albright et al. 2001). These fluctuations might be produced by various mechanisms. At the scale of turbulent motions, they can be generated by the small-scale turbulent MHD dynamo as a result of a series of random stretchings and compressions by the velocity field (e.g., Schekochihin et al. 2002, 2004; Schekochihin & Cowley 2006, and references therein). At microscales of the order of the ion Larmor radius, the ICM plasma is subject to kinetic instabilities (Schekochihin et al. 2005; Schekochihin & Cowley 2006). As the ion Larmor radius is many orders of magnitude smaller than the collisional mean free path, the plasma is weakly collisional, which results in conservation of adiabatic invariants, the first of them being the magnetic moment of a particle $\mu = v_{\perp}^2/(2B)$, where v_{\perp} is the component of the particle velocity perpendicular to the magnetic field. Consequently, the magnetic-field strength changes are correlated with changes in the perpendicular pressure, giving rise to pressure anisotropy. In turn, pressure anisotropy triggers firehose and mirror instabilities (Chandrasekhar et al. 1958; Parker 1958; Hasegawa 1969) that hold the degree of anisotropy $\Delta = (p_{\perp} - p_{\parallel})/p_{\perp}$ at marginal levels $|\Delta| \sim 1/\beta$, where β is the plasma beta, the ratio of thermal to magnetic energy density (for observational evidence in the solar wind, see Kasper et al. 2002; Hellinger et al. 2006; Bale et al. 2009; for theoretical discussion of possible mechanisms of maintaining marginality, see Melville et al. 2015 and references therein). The firehose instability occurs when $\Delta < -2/\beta$, which happens in regions where the field strength is decreasing, near the reversal points of the field lines, and typically generates small ($\delta B_{\perp}/B \ll 1$) transverse Alfvénic fluctuations of the field direction. The mirror instability (or the ‘mirror mode’) is a resonant instability set off when $\Delta > 1/\beta$, which is the case where the field is amplified along the stretches of the field lines. The mirror mode produces fluctuations of magnetic-field strength of order unity ($\delta B/B \sim 1$), which form magnetic traps and may, in principle, inhibit electron transport along the field lines. While field-strength fluctuations $\delta B/B \sim 1$ can also be generated by turbulent motions, we will argue in Section 4 that the resulting suppression of transport is very moderate, because the electron mean free path λ is smaller than the parallel correlation length of the magnetic field l_B , and the electrons can escape from magnetic traps relatively easily. Illustratively, the presumed combined spectrum of magnetic-field strength fluctuations in the ICM is sketched in Fig. 1: the magnetic

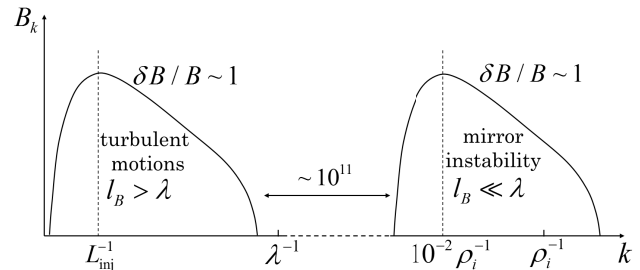


Figure 1. A sketch of the spectrum of the fluctuations of magnetic-field strength in the ICM. The perturbations $\delta B/B \sim 1$ (relevant for magnetic trapping) generated by turbulence occupy the region $\lambda \lesssim l_B$, where magnetic trapping is ineffective. The mirror fluctuations, in contrast, are at the scales comparable to the ion Larmor radius ρ_i , $\lambda \sim 10^{13} \rho_i$, where magnetic mirrors can suppress electron transport considerably.

mirrors capable of efficient suppression of electron transport reside in the region $\lambda \gg l_B$.

The mirror magnetic fluctuations are impossible to observe directly in the ICM due to their extremely small scales, but they can be modeled by numerical simulations. The recent hybrid PIC simulations of the firehose and mirror instabilities in a shearing box done by Kunz et al. (2014) suit this task well in providing the typical statistical properties of the magnetic mirror fluctuations. In this paper, we use the mirror fluctuations produced by their simulations to model the electron motion along the resulting perturbed field lines and estimate the conductivity.

The paper is organized as follows. In Section 2, we describe a model for parallel electron diffusion and its Monte Carlo equivalent for numerical calculations. Then, in Section 3, we apply this model to the mirror magnetic fluctuations taken from the simulations of Kunz et al. (2014) to infer the suppression of parallel electron diffusivity (Section 3.2) and thermal conductivity (Section 3.3). Next, in Section 4, we argue that large-scale turbulent magnetic fluctuations in the ICM, modeled by an isotropic MHD simulation, do not cause a sizable suppression. Finally, in Section 5, we summarize our results and their relevance to the problem of thermal conduction in the ICM and in turbulent weakly collisional plasmas in general.

2 A MODEL FOR PARALLEL ELECTRON DIFFUSION IN A STATIC MAGNETIC FIELD

For our calculations, we assume the electron diffusion timescale to be smaller than the characteristic times of fluid motions and of the magnetic-field evolution, so that the magnetic field can be viewed as static. We will assess the validity of this assumption in Section 5.

If magnetic fluctuations occur at parallel scales l_B much larger than the electron Larmor radius ρ_e , which is indeed true for turbulent magnetic fluctuations, as well as for the mirror-mode perturbations produced at the scale of $1 - 100 \rho_i$, where $\rho_i = (m_i/m_e)^{1/2} \rho_e \sim 40 \rho_e$ is the ion Larmor radius, and if all fluid motions are neglected, we may use the drift-kinetic equation

$$\frac{\partial f}{\partial t} + v\xi\nabla_{\parallel}f - \frac{\nabla_{\parallel}B}{B}v\frac{1-\xi^2}{2}\frac{\partial f}{\partial\xi} = \nu(v)\frac{\partial}{\partial\xi}\frac{1-\xi^2}{2}\frac{\partial f}{\partial\xi}, \quad (1)$$

to evolve the electron distribution function $f = f(t, \mathbf{x}, v, \xi)$ (Kulsrud 1964). Here $\nabla_{\parallel} = \hat{\mathbf{b}} \cdot \nabla$ is the derivative taken along the local magnetic field and $\xi = \hat{\mathbf{b}} \cdot \mathbf{v}/v = \cos\theta$, where θ is the pitch angle. The unit vector $\hat{\mathbf{b}} = \mathbf{B}/B$ points in the local magnetic-field direction. The last term on the left-hand side of equation (1) represents the mirror force, which guarantees conservation of the magnetic moment $\mu = v_{\perp}^2/(2B) = v^2(1-\xi^2)/(2B)$ in the absence of collisions. Isotropic collisions with collision frequency ν are described by the Lorenz pitch-angle scattering operator on the right-hand side of equation (1). In this section, we restrict our analysis to monoenergetic electrons, so there is no energy exchange between the particles. We also neglect the electric field because, close to marginal stability ($\Delta \sim 1/\beta$), the mirror instability generates an electric field of order $E_{\parallel} \sim (T/e)(\nabla_{\parallel}B/B)(1/\beta)$, where T is the electron temperature, e the absolute electron charge. In astrophysical plasmas, β is typically large (e.g., ~ 100 in the ICM), so the electric field can be safely neglected.

The problem is effectively one-dimensional with respect to the arc length ℓ along a field line, because all spatial derivatives in equation (1) are taken along the local magnetic field. Thus, we can rewrite equation (1) in field-aligned coordinates by normalizing the distribution function using the Jacobian of this coordinate transformation, $\tilde{f}(t, \ell, \xi) = f/B$:

$$\frac{\partial \tilde{f}}{\partial t} + \xi \frac{\partial \tilde{f}}{\partial \ell} - M(\ell) \frac{\partial}{\partial \xi} \frac{1-\xi^2}{2} \tilde{f} = \frac{1}{\lambda} \frac{\partial}{\partial \xi} \frac{1-\xi^2}{2} \frac{\partial \tilde{f}}{\partial \xi}, \quad (2)$$

where $M(\ell) = \partial \ln B / \partial \ell$ is the mirror force, $\lambda = v/\nu$ is the electron mean free path¹, and time has been rescaled as $vt \rightarrow t$. Using $\xi = \cos\theta$, the distribution function $F(t, \ell, \theta) = \tilde{f} \sin\theta$ satisfies

$$\frac{\partial F}{\partial t} + \cos\theta \frac{\partial F}{\partial \ell} + \frac{\partial}{\partial \theta} \left[\frac{1}{2} M(\ell) \sin\theta + \frac{\cot\theta}{2\lambda} \right] F = \frac{1}{2\lambda} \frac{\partial^2 F}{\partial \theta^2}. \quad (3)$$

A convenient way to solve this equation by the Monte Carlo method is to treat it as the Fokker-Planck equation for particles whose equations of motions are

$$\begin{aligned} \dot{\ell} &= \cos\theta, \\ \dot{\theta} &= \frac{1}{2} M(\ell) \sin\theta + \frac{\cot\theta}{2\lambda} + \frac{1}{\sqrt{\lambda}} \eta(t), \end{aligned} \quad (4)$$

where $\eta(t)$ is a unit Gaussian white noise, $\langle \eta(t)\eta(t') \rangle = \delta(t-t')$. As clearly seen from these equations, a particle experiences the mirror force $M(\ell)$ defined by the static magnetic field and isotropizing collisions represented by the last two terms on the right-hand side. Equations (4) can be easily solved numerically.

Without collisions, only the particles in the loss cone defined by $|\xi| > (1 - 2\mu B/v^2)^{1/2}$ can travel freely. The rest are reflected by regions of strong field (magnetic mirrors). Collisions allow trapped particles to get scattered into the loss cone and escape from magnetic traps. Oppositely, a free

particle can be knocked out of the loss cone by collisions and become trapped. The key parameter that defines the regime of diffusion is the ratio of the collisional mean free path λ to the parallel correlation length of the magnetic field l_B . If $\lambda/l_B \ll 1$, collisions make magnetic trapping ineffective, and the electrons undergo ordinary diffusion with diffusion coefficient $D \sim \lambda v$. In the opposite limit $\lambda/l_B \gg 1$, collisions are very rare, so the pitch angle changes only slightly over the correlation length of the field. In this regime, the suppression of diffusion is greatest because a certain fraction of the particles is trapped and, in addition, the passing particles have their mean free paths effectively reduced as small-angle collisions cause leakage from the loss cone so that a free particle travels only a fraction of its mean free path before it is scattered out of the loss cone and becomes trapped (Chandran & Cowley 1998; Chandran et al. 1999).

3 ELECTRON DIFFUSION IN A MAGNETIC MIRROR FIELD

3.1 Properties of the mirror field

A description of the numerical code and set-up used to generate the mirror magnetic fluctuations can be found in Kunz et al. (2014). The code (Kunz et al. 2014a) is a hybrid-kinetic particle-in-cell code, in which the electrons are fluid while the ions are treated kinetically as quasi-particles. To trigger the mirror instability, a square 2D region of plasma of spatial extent $L = 1152d_{i0}$, where d_{i0} is the initial ion skin depth, is threaded by a magnetic field directed at an angle to the y -direction and subjected to a linear shear $\mathbf{u}_0 = -Sx\hat{\mathbf{y}}$, which stretches the field lines and, by adiabatic invariance, produces pressure anisotropy. The initial magnetic field strength is B_0 , the initial plasma beta of the ions is taken to be $\beta_0 = 200$, and the shear is $S = 3 \times 10^{-4} \Omega_i$, where Ω_i is the ion gyrofrequency. The ion Larmor radius is $\rho_i = \sqrt{\beta} d_i$. Once the (ion) pressure anisotropy $\Delta = p_{\perp}/p_{\parallel} - 1$ reaches $1/\beta$, the plasma becomes mirror-unstable. Magnetic perturbations grow exponentially until they become large enough to drive the anisotropy back to the marginal level, $\Delta \rightarrow 1/\beta$. Persistent large-scale driving of the pressure anisotropy, coupled with the requirement for the plasma to remain marginally stable, leads to a long phase of secular growth of the mirror perturbations. The spatial structure of the perturbations during this phase is shown in Fig. 2. The mirror fluctuations are elongated in the direction of the mean magnetic field and have $\delta B_{\parallel} \gg \delta B_{\perp}$. During this secular phase, the field grows as $\delta B \propto t^{4/3}$ and the dominant modes shift towards longer wavelengths ($k_{\parallel} \rho_i \sim 10^{-2}$) as the pressure anisotropy asymptotically approaches marginal stability. The marginal stability is achieved and maintained during the secular phase by the trapping of ions in magnetic mirrors (see Rincon et al. 2015; Melville et al. 2015). The final saturation sets in when $\delta B/B_0 \sim 1$ at $St \gtrsim 1$, and is caused by the enhanced scattering of ions off sharp ($\delta B_{\parallel}/B_0 \sim 1$, $k_{\parallel} \rho_i \sim 1$) bends in the magnetic field at the edges of the mirrors.

We note that the electrons in the code are isothermal with $T_e = T_i$, so we are not attempting to solve the problem of the electron heat transfer self-consistently (no thermal gradients and heat fluxes are present). We have

¹ Electron collisionality may be anomalous due to, e.g., scattering off magnetic fluctuations generated by electron microinstabilities. This could reduce the effective electron mean free path, but our main results would remain valid as long as the effective mean free path is much larger than the ion Larmor scale.

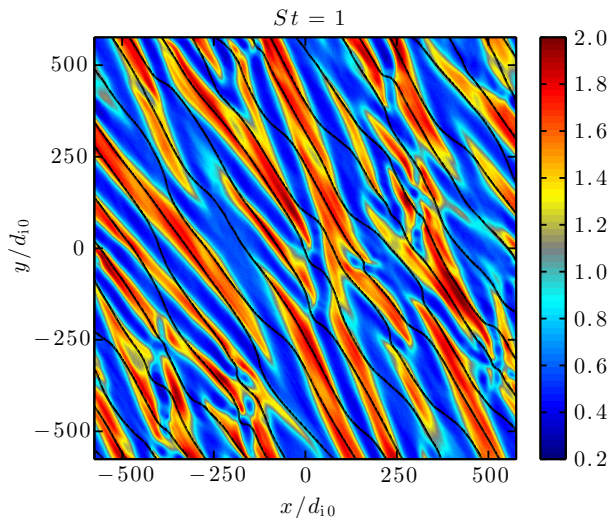


Figure 2. Spatial structure of the mirror instability (Kunz et al. 2014) during the secular phase of the perturbations’ growth, after one shear time. The magnetic-field strength $B/\langle B \rangle$ is shown by color, the field lines are shown by contours. Length is in the units of the ion skin depth $d_{i0} = \rho_i(St = 0)/\sqrt{\beta_0}$. At time $St = 1$, the ion Larmor radius is $\rho_i \approx 8.7d_{i0}$.

extracted two representative magnetic-field lines from the simulation domain, one during the secular phase ($St = 1$), and one during the saturated phase ($St \approx 1.8$). Each of these crosses the box 8 times (note that, although the box is shearing-periodic, a field line does not bite its tail and hence can be followed over several crossings) and has a length of $\approx 18000d_{i0}$ (we adopt d_{i0} as our unit of length because d_i is practically constant in time, while ρ_i is a function of the field strength). The variation of the magnetic-field strength B along the lines is shown in Fig. 3. From the analysis of the probability density functions (PDF) of B for the two field lines (Fig. 4), it is clear that in both cases, the PDFs have abrupt cut-offs at large $B \sim$ several B_0 , as well as at small B . Therefore, the field is bounded with no large deviations from the mean value, in contrast to, e.g., a lognormal stochastic magnetic field with the same rms (shown by the dotted line in Fig. 4 for comparison) with a tail in its PDF, for which there is always a non-zero probability to find a large deviation at a large enough scale. This also means that the extracted field lines fully represent the statistics of B (a longer field line would not contain more statistical information). The bounded PDF(B) is a key property of the mirror magnetic field, which leads to a finite value of suppression of electron transport at large λ/l_B , unlike in the case of stochastic magnetic fields (lognormal, Gaussian, exponential) that can completely inhibit particle transport in this limit (Mal’yskin & Kulsrud 2001; Albright et al. 2001).

3.2 Suppression of electron diffusivity in the limit $\lambda/l_B \gg 1$

3.2.1 Results of the Monte Carlo simulations

For the two extracted field lines, we integrate the particles’ trajectories defined by equations (4) numerically. Initially, the particle distribution is isotropic with the particle density

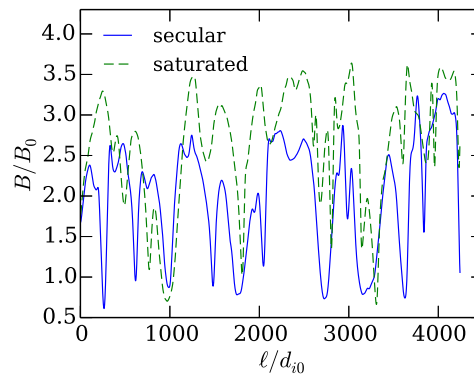


Figure 3. Variation of the magnetic-field strength along a field line during the two different phases of evolution of the mirror fluctuations (*solid*: secularly growing fluctuations at time $St = 1$; *dashed*: saturated fluctuations at time $St \approx 1.8$). B_0 is the initial magnetic-field strength in the simulation. For convenience, 4000- d_{i0} line segments are shown. The ion Larmor radii are $\rho_i(St = 1) \approx 8.7d_{i0}$ and $\rho_i(St \approx 1.8) \approx 6.2d_{i0}$.

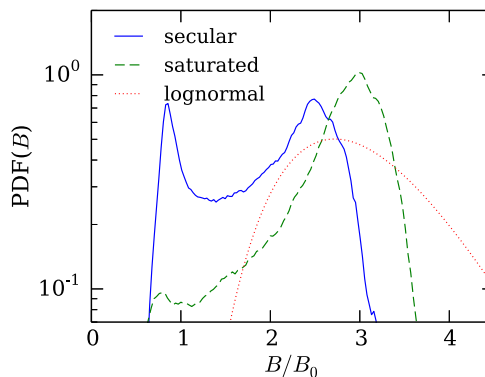


Figure 4. PDFs of the magnetic-field-strength fluctuations generated by the mirror instability. A lognormal distribution with rms equal to the rms of the logarithm of the saturated mirror fluctuations is shown by the dotted line for comparison.

along a field line set to $\propto 1/B$, which is a uniform density distribution in real space [recall the Jacobian of the coordinate transformation to field-aligned coordinates in equation (2)]. Then we trace the evolution of the particles over time $t_1 = 20 t_{\text{coll}}$, where $t_{\text{coll}} = 1/\nu$ is the collision time. The monoenergetic diffusion coefficient D is calculated as

$$D = \frac{\langle [\ell_i(t_1) - \ell_i(t_0)]^2 \rangle}{2(t_1 - t_0)}, \quad (5)$$

where ℓ_i are the particles’ displacements. We choose $t_0 = 5 t_{\text{coll}}$ in order to allow the particles to collide a few times until the ballistic regime gives way to diffusion at $t \gtrsim t_{\text{coll}}$. The same procedure is carried out for several different ratios λ/l_B in the range $2 \cdot 10^{-4} - 5 \cdot 10^4$. The correlation lengths of the field strength along the lines are $l_B \approx 850d_{i0} \approx 100\rho_i(St = 1)$ for the secular phase and $l_B \approx 1430d_{i0} \approx 230\rho_i(St \approx 1.8)$ for the saturated phase.

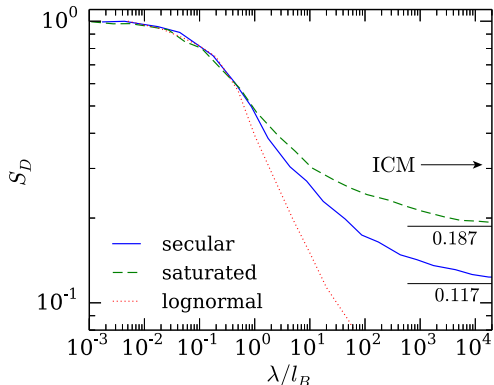


Figure 5. Suppression factor of the electron diffusivity $S_D = D/D_0$ in the secularly growing (solid line) and saturated (dashed line) magnetic fluctuations. The correlation lengths of the field strength along the field lines are $l_B \approx 850d_{i0} \approx 100\rho_i$ ($St = 1$) during the secular phase and $l_B \approx 1430d_{i0} \approx 230\rho_i$ ($St \approx 1.8$) for the saturated mirrors. For comparison, the dotted line shows suppression in a synthetic lognormal magnetic field with the same rms value of $\log B$ as during the phase of secular growth of the mirror fluctuations, correlation length $l_B = 850d_{i0}$ and a Kolmogorov spectrum in space (see its PDF in Fig. 4).

Defining $D_0 = (1/3)\lambda v$, the diffusion coefficient in the absence of the magnetic fields, we thus obtain the monoenergetic diffusion suppression factor $S_D = D/D_0$ as a function of λ/l_B (Fig. 5). Averaging the monoenergetic diffusivity D over a thermal distribution of the electron speeds v introduces only a slight change in the shape of the function $S_D(\lambda/l_B)$, so we only present the monoenergetic diffusion suppression in what follows.

For magnetic mirror fluctuations in the ICM, the limit $\lambda/l_B \gg 1$ is the relevant one, because the ion Larmor radius is many orders of magnitude smaller than the mean free path:

$$\lambda \approx 20 \text{ kpc} \left(\frac{T}{8 \text{ KeV}} \right)^2 \left(\frac{n}{10^{-3} \text{ cm}^{-3}} \right)^{-1}, \quad (6)$$

$$\rho_i \approx 5 \times 10^{-12} \text{ kpc} \left(\frac{T}{8 \text{ KeV}} \right)^{1/2} \left(\frac{B}{1 \mu\text{G}} \right)^{-1}. \quad (7)$$

In this limit, the suppression factor asymptotically approaches $S_D \approx 0.12$ during the secular phase, and $S_D \approx 0.19$ for the saturated mirrors. The absence of the mean-free-path dependence at large λ/l_B is due to the fact that the mirror fluctuations are bounded, as we have seen by analyzing their PDF (Fig. 4). This is very different from the case of stochastic magnetic mirrors (see Malyshkin & Kulsrud 2001; we will discuss stochastic magnetic mirrors in more detail in Section 4.1).

3.2.2 The role of the PDF(B)

The limiting values of S_D in Fig. 5 depend only on the PDF(B) along the field lines. This fact is intuitive because the change in the pitch angle of a passing particle due to collisions as it travels the correlation length l_B of the field is very small, and the order in which the particle encoun-

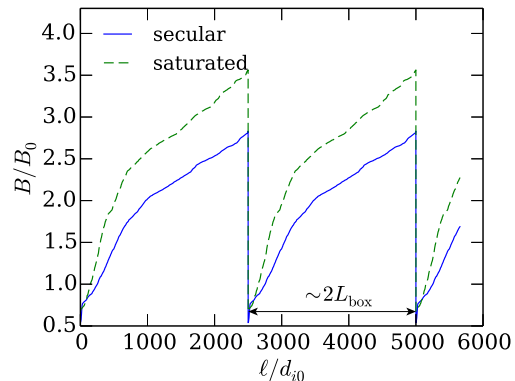


Figure 6. Equivalent representation of the mirror magnetic fluctuations along the field lines in the case $\lambda/l_B \gg 1$. Reordering the magnetic-field strength values over length $L \sim 2L_{\text{box}}$, $l_B \lesssim L \ll \lambda$, does not change the PDF(B) and, therefore, the amount of diffusion suppression.

ters regions of different B plays no role. Therefore, one can rearrange the mirror magnetic fluctuations (Fig. 3) by sorting the array elements in ascending order over some length L , $l_B \lesssim L \ll \lambda$, and making the resulting array periodic with period L (Fig. 6). Since the field is bounded, we do not lose statistical information if L is set to just a few l_B . Clearly, this procedure keeps the PDF(B) unchanged, and the resulting magnetic field produces the same amount of suppression, while having a much simpler shape. By comparing such simplified shapes of magnetic fluctuations for different field lines, one can determine which line causes more suppression. The loss cone for a particle is defined as $|\xi| > (1 - B/B_{\text{max}})^{1/2}$, where B is the magnetic-field strength at the location of the particle and B_{max} is the global maximum of the field strength. The more concave (or less convex in our case of the mirror fluctuations) the shape is, the more suppression is produced by magnetic mirroring, because the loss cones of most of the particles become narrower. The extreme case of this is a field that consists of narrow periodic peaks of height $B_{\text{max}} - B_{\text{min}}$. This field causes maximum suppression of diffusion for given values of B_{min} and B_{max} , because the loss cone for almost all the particles, $|\xi| > (1 - B_{\text{min}}/B_{\text{max}})^{1/2}$, is the narrowest it can be for all possible PDF(B). Based on this argument, and noticing that, in Fig. 4, the PDF of the saturated mirror field is more concentrated around the maximum field strength, one can predict more suppression of electron diffusion by secularly growing mirrors than by saturated ones, even though B_{max} is smaller for the former than for the latter. Indeed, we see in Fig. 5 that the effect of the field shape prevails over the difference in B_{max} , and the diffusion suppression is stronger for the secular phase.

3.2.3 The physical mechanism of the suppression of electron diffusion at large λ/l_B

In the limit $\lambda/l_B \gg 1$, Chandran et al. (1999) derived an analytic expression for the suppression of diffusivity of monoenergetic electrons by periodic magnetic mirrors [their equation (95)]:

$$S_D = \frac{3}{\langle 1/B' \rangle} \int_0^1 d\mu'_1 \int_{\mu'_1}^1 d\mu'_2 \frac{1}{\langle |\xi(\mu'_2)|/B' \rangle}, \quad (8)$$

where $B' = B/B_{\max}$ is the magnetic-field strength normalized to its global maximum value, $\mu' = \mu/\mu_{\text{crit}}$ is the magnetic moment of a particle $\mu = v^2(1 - \xi^2)/(2B)$ normalized to $\mu_{\text{crit}} = v^2/(2B_{\max})$, the averaging is performed over the period of the magnetic field, and the integration is carried over the passing particles in the loss cone. As we have discussed in Section 3.2.2, bounded mirror fluctuations can be replaced by periodic variations with the same PDF(B) without affecting the suppression factor. This means that equation (8), where the averaging in the angle brackets is done over PDF(B), can be readily applied to the simulated mirror fluctuations. The asymptotic values of S_D calculated by equation (8), $S_D \approx 0.117$ for the secularly growing mirrors and $S_D \approx 0.187$ for the saturated ones, agree extremely well with the results of our Monte Carlo simulation (see Fig. 5).

We can break down the suppression effect encoded in equation (8) into two physical effects:

$$S_D = S_p \frac{\lambda_{\text{eff}}}{\lambda}, \quad (9)$$

where S_p is the suppression of diffusivity due to the fact that only the passing particles contribute to electron transport, λ_{eff} is the effective mean free path of the passing particles, reduced because a passing particle is scattered out of the loss cone, becomes trapped and randomizes its direction of motion in only a fraction of its collision time. The parameters S_p and λ_{eff} have a very clear physical interpretation in terms of the particle velocity autocorrelation function.

The electron diffusion coefficient D can be expressed as the integral of the parallel-velocity autocorrelation function $C(t)$:

$$D = \int_0^\infty \langle v_{\parallel}(0)v_{\parallel}(t) \rangle dt \equiv \int_0^\infty C(t) dt. \quad (10)$$

Using the results of our Monte Carlo simulations of monoenergetic diffusion in magnetic fluctuations generated by the mirror instability, we can calculate the parallel-velocity autocorrelation function, which is, for monoenergetic electrons, the autocorrelation function of the cosine of the pitch angle $\xi = \cos\theta$, namely $C(t) = v^2 \langle \xi(0)\xi(t) \rangle$. It is plotted in Fig. 7 for diffusion with no magnetic mirrors (dashed line) and diffusion in the mirror magnetic field with $\lambda/l_B = 100$ (solid line). With no mirrors,

$$C_0(t) = \frac{1}{3} v^2 e^{-\nu t}, \quad (11)$$

where $\nu = v/\lambda$. Both with or without mirrors, the autocorrelation function is equal to $1/3$ at $t = 0$ due to isotropy (even in the presence of magnetic mirrors, collisions restore isotropy over times $\gg \nu^{-1}$). In the mirror field, $C(t)$ has a narrow peak of width $\sim l_B/v$ at small t , while the rest of the autocorrelation function is an exponential that is well fitted by

$$C(t > l_B/v) = \frac{1}{3} S_p v^2 e^{-\nu_{\text{eff}} t}, \quad (12)$$

where $S_p < 1$ and $\nu_{\text{eff}} > \nu$.

The narrow peak of $C(t)$ at small t is caused by the contribution to $C(t)$ of the population of trapped particles, which bounce inside magnetic traps at a typical time scale $\sim l_B/v$. The physical meaning of the reduction factor $S_p <$

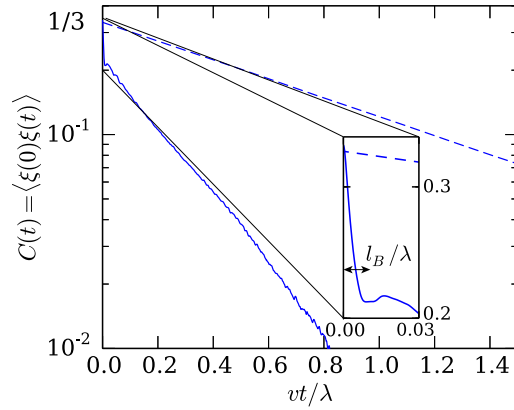


Figure 7. The parallel velocity autocorrelation functions $C(t)/v^2$ for electron diffusion in a constant magnetic field (dashed) and in the magnetic field of secularly growing mirrors (solid), based on the results of the Monte Carlo simulation. The ratio of the electron mean free path to the correlation length of the magnetic field $\lambda/l_B = 100$. The narrow peak at $t < l_B/v$ is caused by the bouncing trapped particles, which do not contribute to electron transport.

1 is that only the passing particles contribute to transport processes. This factor can be calculated as

$$S_p = f_{\text{pass}} \frac{\langle \xi^2 \rangle_{\text{pass}}}{\langle \xi^2 \rangle}, \quad (13)$$

where f_{pass} is the fraction of the passing particles, the averaging is performed over the passing particles in the numerator, and over all particles in the denominator. The value of S_p is greater than simply the fraction of the passing particles, because they travel in their loss cones and, therefore, have parallel velocities greater than the mean square parallel velocity $v^2 \langle \xi^2 \rangle = v^2/3$ averaged over all particles.

The physical interpretation of the fact that $\nu_{\text{eff}} > \nu$ in equation (12) is the reduced effective mean free path of the passing particles: recall that a passing particle travels only a fraction of λ before it becomes trapped and, obviously, $\nu_{\text{eff}}/\nu = \lambda/\lambda_{\text{eff}}$. Since the diffusion coefficient is the integral of $C(t)$ [equation (10)], we obtain equation (9).

From the above arguments, it follows that a system with magnetic mirrors and $\lambda/l_B \gg 1$ can be translated into a system with no mirrors, but with a lower mean square parallel velocity and an enhanced scattering rate. The lower parallel velocity is related to the fact that the passing particles become trapped now and then, and while they are trapped, their effective parallel velocity is zero.

Using the results of our Monte Carlo simulations and the velocity autocorrelation function analysis described above, we can measure S_p and $\lambda_{\text{eff}}/\lambda$. For the secularly growing mirrors, we get $S_p \approx 0.63$, $\lambda_{\text{eff}}/\lambda \approx 0.19$; for the saturated mirrors, $S_p \approx 0.74$, $\lambda_{\text{eff}}/\lambda \approx 0.26$. Substituting these into equation (9), we recover $S_D \approx 0.12$ and $S_D \approx 0.19$, the same as was obtained in direct measurement [equation (5)] and from equation (8).

3.3 Suppression of electron thermal conductivity in the limit $\lambda/l_B \gg 1$

As we have shown above, the effect of magnetic mirrors on scales much larger than the electron mean free path is the suppression of spatial diffusion via two effects: reduced fraction and reduced effective mean free path (or, equivalently, an enhanced scattering rate) of the passing particles participating in transport [see equation (9)]. In a plasma with a temperature gradient and no mirrors, heat transport is governed not only by pitch-angle diffusion, but by diffusion in the energy space as well. Magnetic mirrors do not change a particle's energy, therefore, one can model their effect on large scales by enhancing the pitch-angle scattering rate (but not the energy diffusion rate) and, simultaneously, reducing the effective density of particles carrying energy in order to subtract the trapped population.

The rates of pitch-angle scattering (perpendicular velocity diffusion) ν_\perp and energy exchange ν_ε for a test electron in a hydrogen plasma are (Spitzer 1962)

$$\nu_{\perp,es} = 2[(1 - 1/2x)\psi(x) + \psi'(x)]\nu_0, \quad (14)$$

$$\nu_{\varepsilon,es} = 2[(m_e/m_s)\psi(x) - \psi'(x)]\nu_0, \quad (15)$$

where

$$\nu_0 = \frac{4\pi e^4 \ln \Lambda n_e}{m_e^2 v^2}, \quad x = v^2/v_{th,e}^2, \quad (16)$$

$$\psi(x) = \frac{2}{\sqrt{\pi}} \int_0^x dt \sqrt{t} e^{-t}, \quad \psi'(x) = \frac{d\psi}{dx}, \quad (17)$$

$s = e, i$ is the species of the background particles, $v_{th,e} = (2kT_e/m_e)^{1/2}$ is the electron thermal speed, and $\ln \Lambda \sim 40$ is the Coulomb logarithm. Heat is transferred by slightly superthermal electrons with $v \approx 2.5 v_{th,e}$ (this rough estimate is based on a simple calculation of thermal conductivity for a Lorenz gas, when electrons interact only with ions). At this velocity, $\nu_{\perp,ei} \approx 1.5 \nu_0$, $\nu_{\perp,ee} \approx 1.8 \nu_0$, $\nu_\varepsilon = \nu_{\varepsilon,ei} + \nu_{\varepsilon,ee} \approx \nu_{\varepsilon,ee} \approx 2 \nu_0$. Thus, the electron energy exchange rate ν_ε is close to the total perpendicular electron diffusion rate $\nu_\perp \approx 3.3 \nu_0$ for the heat-conducting electrons.

At this point, we make a qualitative assumption that the total rate of spatial energy transfer can be reasonably approximated by the sum of the energy exchange rate and the pitch-angle scattering rate. This assumption is corroborated by the mathematical fact that in a plasma with a gradient of a diffusing passive scalar, the flux of the scalar is inversely proportional to the sum of the rate of spatial diffusion of the particles (or pitch-angle scattering) and the collisional exchange rate of the passive scalar [see Appendix A, equation (A11)]. The passive scalar in this calculations models temperature, as if every particle carried an averaged value of thermal energy that did not depend on the particle's velocity. Then for the thermal conductivity κ , we use the approximation

$$\kappa \sim \frac{\nu_{th,e}^2}{\nu_\varepsilon + \nu_\perp}. \quad (18)$$

The reduction of the effective density of the heat-conducting electrons affects both pitch-angle and energy diffusion, while the enhanced scattering rate only affects pitch-angle diffusion. Thus, the suppression of thermal conduction is smaller than the suppression of spatial diffusion. A quali-

tative expression for the suppression of thermal conductivity $S_\kappa = \kappa/\kappa_0$ in the limit $\lambda/l_B \gg 1$ is then

$$S_\kappa \sim S_p \frac{\nu_\perp + \nu_\varepsilon}{(\lambda/\lambda_{eff})\nu_\perp + \nu_\varepsilon} \sim \frac{2S_p}{1 + \lambda/\lambda_{eff}}, \quad (19)$$

where S_p and λ_{eff} are the parameters in equation (9): S_p is related to the fraction of the passing particles, λ_{eff} is the effective mean free path of the passing particles. For a passive scalar in the limit $\lambda/l_B \gg 1$, equation (19) is exact and derived in Appendix A by establishing a simple relationship between the amount of suppression of the scalar flux and the parallel-velocity autocorrelation function. Substituting the values of S_p and λ_{eff}/λ calculated at the end of Section 3.2.3 into equation (19), we obtain the suppression factor of thermal conductivity: $S_\kappa \sim 0.2$ for the secularly growing mirrors and $S_\kappa \sim 0.3$ for the saturated ones. We see that heat transport is suppressed by a factor of ~ 2 less than spatial diffusion, because the diffusion in energy space is suppressed much less than the spatial (pitch-angle) diffusion. Equation (19) can only be used when S_p and λ_{eff} do not depend on the electron velocity (or, equivalently, on the electron mean free path λ), which is indeed the case in the limit $\lambda/l_B \gg 1$ (see Fig. 5).

4 ELECTRON TRANSPORT IN MHD TURBULENCE

As mentioned in Section 1, another source of fluctuations of magnetic-field strength in the ICM is turbulent stretching/compression of the field lines. The turbulent dynamo produces a stochastic distribution of the field strength along a field line: lognormal during the kinematic phase, exponential in saturation (see Schekochihin et al. 2004). However, as we have also noted in Section 1, we do not expect much suppression of thermal conduction by these fields, because the electron mean free path is smaller than the parallel correlation length of turbulent magnetic fluctuations, and so magnetic mirrors are rare and not very effective. In this section, we demonstrate this explicitly by means of an isotropic MHD simulation of turbulent dynamo.

4.1 Suppression of electron transport in a system of stochastic magnetic mirrors

Before we consider the magnetic fields produced by the turbulent MHD dynamo, let us first illustrate how different diffusion in a stochastic magnetic field is from the case of a periodic field (characteristic of the mirror fluctuations) by the example of a lognormally distributed field. A stochastic magnetic field with a long tail in its PDF produces a larger amount of suppression compared to periodic magnetic fluctuations, because the dominant suppression is caused by the so-called 'principal magnetic mirrors' of strength $m_p = B_p/\langle B \rangle \gg 1$ separated from each other by a distance of order the effective mean free path (characteristic length that a passing particle travels before it gets scattered out of the loss cone and becomes trapped) λ/m_p (Malyshkin & Kulsrud 2001). Because $\lambda/m_p \gg l_B$ (see Malyshkin & Kulsrud 2001 for a calculation of m_p), the principal mirrors arise at scales much larger than l_B and therefore are strong deviations of

the field strength from the mean value found in the tail of the PDF.

We generate a lognormal magnetic field with a Kolmogorov spectrum and the same rms value of the logarithm of the field strength and the same correlation length l_B as the secularly growing mirror fluctuations analyzed in Section 3 (the dotted PDF in Figure 4). The diffusivity suppression factor is obtained by a Monte Carlo simulation and shown in Figure 5 by the dash-dotted line. Its dependence on λ/l_B is much steeper than for the mirror fields, with no constant asymptotic value at large λ/l_B . Qualitatively, it is quite similar to the effective suppression of conductivity obtained for stochastic distributions by Malyshkin & Kulsrud (2001, see their Fig. 3).

4.2 Suppression of electron transport in a saturated magnetic field produced by MHD dynamo.

We have demonstrated that the suppression of electron diffusion in a stochastic field may be considerably larger than in a mirror-like periodic field, most notably if $\lambda \gg l_B$. However, this regime is inapplicable to the magnetic fluctuations generated by MHD turbulence in the ICM, because there $\lambda \lesssim l_\nu < L_{\text{inj}} \sim l_B$, where l_ν is the viscous scale of turbulent eddies, L_{inj} the outer (injection) scale of turbulence, and l_B is the *parallel* correlation length of the magnetic field. While MHD-dynamo-produced magnetic fluctuations decorrelate at small (resistive) scales, it is the field's variation perpendicular to itself (direction reversals) that occurs at those scales, whereas the parallel variation is on scales l_B of order the flow scale $L_{\text{inj}} \gg \lambda$ (Schekochihin et al. 2002, 2004). In the cool cores of galaxy clusters, $\lambda \sim 0.05$ kpc, $l_\nu \sim 0.4$ kpc, $L_{\text{inj}} \sim 10$ kpc (based on the parameters for the Hydra A cluster given by Enßlin & Vogt 2006); in the hot ICM, $\lambda \sim 20$ kpc, $l_\nu \sim 100$ kpc, $L_{\text{inj}} \sim 200$ kpc. Schematically, the spectrum of magnetic-field-strength fluctuations in the ICM is shown in Figure 1. In order for magnetic trapping to be effective, magnetic-field-strength fluctuations $\delta B/B \sim 1$ need to exist at spatial scales below the electron mean free path. While mirror fluctuations easily satisfy this condition, MHD turbulence capable of creating parallel magnetic fluctuations occupies scales above λ , so large suppression is not expected in this case.

In order to estimate an upper limit on the suppression of electron diffusion by MHD magnetic fluctuations, we use simulations of a turbulent MHD dynamo at different magnetic Prandtl numbers $\text{Pm} = \nu/\eta$, where ν is the fluid viscosity, η the magnetic diffusivity. Our code solves the full set of compressible MHD equations in 3D, and is based on the unsplit van Leer integrator combined with the constrained transport (CT) method, similar to the one implemented in *ATHENA* (Stone & Gardiner 2009). We initiate a 3D 256^3 periodic box of MHD plasma with magnetic fluctuations at the level $\beta = 2000$, and stir it by a random white-in-time nonhelical body force applied at the largest scales ($L_{\text{inj}} \sim$ the box size). As we noted earlier in this section, the smaller the ratio λ/L_{inj} is, the less effective magnetic trapping is. In terms of the Reynolds number $\text{Re} \sim L_{\text{inj}} u / \lambda \nu_{\text{th},i}$, it means that for small Ma/Re , where Ma is the Mach number of the turbulent motions, conduction suppression should be negligible. In the cores of galaxy clusters, $\text{Re} \sim 100$ (Hydra A),

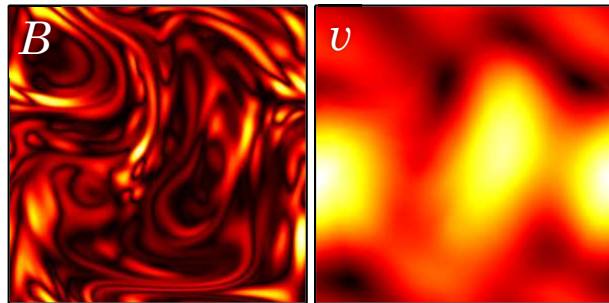


Figure 8. Central snapshot of cross-sections of a dynamo-generated magnetic-field (*left*) and velocity (*right*) magnitudes during the saturated turbulent MHD state for $\text{Pm} = 1000$, $\text{Re} = 3$.

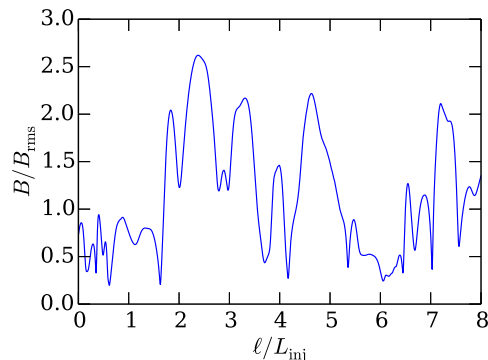


Figure 9. Variation of the magnetic-field strength along a field line segment that spans 8 boxes (box size = energy injection scale L_{inj}), taken from an MHD simulation of the saturated state of turbulent dynamo at $\text{Pm} = 1000$, $\text{Re} = 3$.

while in the bulk of the ICM, $\text{Re} \sim 1 - 10$ (ignoring the possible effects of microinstabilities on the gas viscosity). The typical Mach number in galaxy clusters is believed to be $\text{Ma} \sim 0.1$ (e.g., Zhuravleva et al. 2015). Because we seek to obtain an upper limit on suppression, we restrict our analysis to low Re , corresponding to the hot ICM (at such low Re , turbulence will not have a wide inertial range, but that is irrelevant because turbulent MHD dynamo only requires a stochastic velocity field, not necessarily a fully developed Kolmogorov turbulence). Namely, in our simulation, we use $\text{Re} = 3$, and $\text{Pm} = 1000$. The simulation lasts until the magnetic field becomes saturated: $\langle B^2 \rangle / (8\pi) \sim \langle \rho v^2 \rangle / 2$, where ρ is the mass density, v the turbulent plasma flow velocity (in saturation, $\beta \sim 50$ and $\text{Ma} \sim 0.1$). The structure of the magnetic and velocity fields in the saturated state is shown in Figure 8: magnetic folds are clearly seen at the scale of the box, while the velocity is stochastic but smooth, due to low Re . This simulation setup and the properties of the saturated magnetic field are similar to those of the run "S4-sat" in Schekochihin et al. (2004).

Following the same strategy as in the case of the mirror fields, we have extracted a magnetic-field line from the box in the saturated state. The extracted field line spans 100 box sizes (again, a field line does not bite its tail, although the box is periodic). This is necessary to make it statisti-

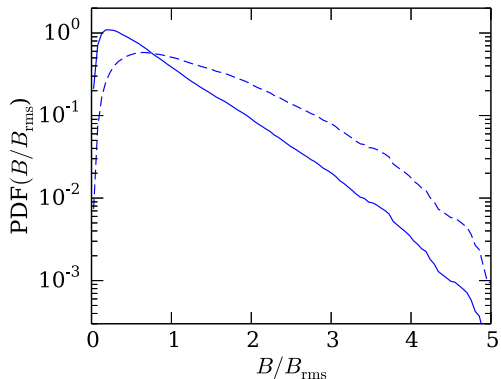


Figure 10. *Solid line:* the 3D PDF of the magnetic-field strength in saturated state for $Pm = 1000$, $Re = 3$. *Dashed line:* the PDF of B along the field line (the 3D PDF multiplied by B).

cally representative, because the PDF of the field now has an exponential tail. A line segment that spans 8 boxes is shown in Figure 9. The PDF of the magnetic-field strength calculated over the whole 3D simulation domain and one calculated along the field (by multiplying the 3D PDF by the magnetic-field strength) are shown in Figure 10. They clearly exhibit an exponential shape. We calculate the suppression of electron diffusion in the same way as we did for the mirror fields in Section 3.2.1. The suppression factor is shown in Figure 11 as a function of the ratio of the the mean free path λ to the injection scale L_{inj}^2 . For the fiducial parameters of the hot ICM with the largest value of λ , we choose $L_{inj} \sim 200$ kpc and $\lambda \sim 20$ kpc. These parameters provide maximum suppression factor of electron diffusion $S_D \sim 0.9$. It is shown in Figure 11 by the cross, the solid line corresponds to the suppression factor at lower λ , while the dashed line shows this factor for test monoenergetic electrons at higher λ to better exhibit the shape of the function $S_D(\lambda/l_B)$ for the dynamo-generated magnetic field. Though in this case, there is no simple connection between diffusivity and thermal conductivity [like equation (19)], because S_D now strongly depends on the mean free path (or velocity), the suppression of thermal conduction for $\lambda \lesssim 20$ kpc should be essentially insignificant.

5 DISCUSSION

It is well recognized that thermal conduction in the ICM is anisotropic in the presence of even an extremely weak magnetic field. A popular assumption, adopted in many theoretical and numerical studies, is that conduction is suppressed across the field, while along the field, it is equal to the isotropic thermal conduction in an unmagnetized plasma. This assumption is typically applied to large-scale fields in the ICM, e.g., to scales of order 10 kpc, which correspond to the characteristic field correlation length inferred from Faraday rotation measurements (e.g., Kuchar & Enßlin 2011).

² Note that this is a somewhat artificial parameter scan as we do not vary the ion mean free path, i.e., the viscosity, in a manner consistent with the electron mean free path.

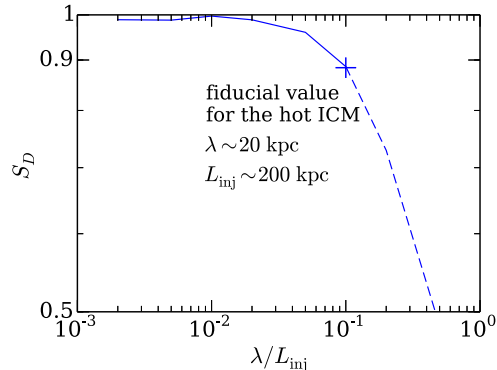


Figure 11. The suppression factor $S_D = D/D_0$ of the electron diffusivity by turbulent-dynamo-produced magnetic fields. The cross indicates the largest possible suppression for the fiducial parameters of the hot ICM: $L_{inj} \sim 200$ kpc, $\lambda \sim 20$ kpc.

However, the ICM is likely to be susceptible to microinstabilities on much smaller scales comparable with the ion Larmor radius. In particular, the mirror instability can generate fluctuations of the field strength of large amplitude $\delta B/B \sim 1$, which can partially suppress electron transport along the field lines. Given that the ion Larmor radius is some 13 orders of magnitude smaller than the typical macroscopic scales, small-scale magnetic mirrors could potentially modify thermal conduction in a significant way, provided that mirrors can trap the electrons.

To address this question, we have examined the properties of the field-strength fluctuations in the recent shearing-box simulations of the mirror instability by Kunz et al. (2014). The striking difference between the magnetic fluctuations produced in these simulations and a generic random field is that their $PDF(B)$ has sharp cutoffs at both low and high B , with the ratio of the maximal and minimal field strengths over the field lines $B_{max}/B_{min} \sim 6-7$. Since the ratio $B_{max}/B(\ell)$ determines the loss cone for a particle at the location ℓ along the line, the modest values of B_{max}/B_{min} already suggest a limited amount of suppression, although it depends also on the exact shape of the $PDF(B)$ (see Section 3.2.2).

Indeed, in our Monte Carlo simulations, we have found that the electron diffusivity is suppressed by a factor of ~ 8 for secularly growing mirrors and by a factor of ~ 5 for saturated ones. A lognormal magnetic field with the same rms would produce a much stronger suppression. We further argue that the suppression of thermal conduction relative to an unmagnetized plasma is a factor of ~ 2 less strong due to the fact that mirrors primarily affect spatial transport of the electrons, and much less the energy equilibration time. We conclude that microscale magnetic mirrors give rise to a factor of ~ 5 suppression of the parallel thermal conductivity.

In this work, we assumed a static magnetic field taken from a region of a plasma where the field lines are stretched by a linear shear. Though at a given location in the ICM plasma, the field lines are not constantly stretched, the turbulent dynamo produces a magnetic-field-line configuration that consists of long folds (regions of amplified field)

and short reversals (regions of decreasing/weak field). This means that mirror fluctuations may develop almost everywhere along the field lines in a turbulent ICM (see Rincon et al. 2015 for the first numerical evidence of this). We note that it is not yet known how the mirror and firehose instabilities evolve over multiple correlation times of a turbulent velocity field. However, the recent results by Melville et al. (2015) indicate that at the values of β typical for the ICM, the relaxation of pressure anisotropy in a changing macroscale velocity shear is almost instantaneous compared to the shear time. This may therefore suggest that the mirror instability does not have time to ever reach the saturated state (at $St \gtrsim 2$ according to Kunz et al. 2014), because the turbulent shear decorrelates earlier (at $St \sim 1$). Thus, secularly growing mirrors are expected to be more common. In any case, since the results for both phases are similar up to a factor of order unity, we do not expect large deviations from the described above behavior. We may then argue that the amount of suppression found using the shearing-box simulations is characteristic for the ICM or any other turbulent weakly collisional high- β plasma.

When the parallel scale of the field is larger than the particles' mean free path, the suppression of conductivity is not strong because collisions are frequent enough to stop particle trapping. This means that even though macroscopic MHD turbulence can produce large-scale variations of B , the resulting suppression of parallel conduction should be negligible. We illustrate this point by carrying out MHD simulations of saturated turbulent dynamo and explicitly calculating the suppression factor (Section 4.2).

Parallel thermal conduction can also be reduced by anomalous pitch-angle scattering of electrons off magnetic perturbations. Such perturbations can be produced at the scale of the electron Larmor radius by the whistler instability triggered by electron pressure anisotropy (Riquelme et al. 2016). In the ICM, Riquelme et al. (2016) estimate the resulting effective electron mean free path to be at most a few times smaller than the Coulomb mean free path, so our results remain valid (the mean free path is still much larger than the ion Larmor scale). The additional electron scattering will cause additional suppression of thermal conduction. The suppression by the mirror instability should then be our factor of $S_D \sim 1/5$ relative to this whistler-modified conductivity.

In addition to the suppression of parallel thermal conduction, the stochastic topology of the magnetic-field lines contributes to the total suppression of the global large-scale thermal conductivity by making the path travelled by an electron longer. When studying this effect, the effective increase of transverse diffusion due to the exponential divergence of the stochastic field lines should be taken into account (e.g., Rechester & Rosenbluth 1978), because it restores the diffusive regime of spatial particle transport. If magnetic turbulence develops over a range of scales, the suppression effect is quite modest, $\sim 1/5$ of the Spitzer value (Narayan & Medvedev 2001; Chandran & Maron 2004). Since we have shown that the parallel conductivity is suppressed by another factor of ~ 5 ,

we argue that the global large-scale thermal conduction in the ICM is roughly $\sim 1/20 - 1/30$ of the Spitzer value.³

ACKNOWLEDGEMENTS

We thank S. C. Cowley for helpful discussions. The authors are grateful to W. Pauli Institute, Vienna, for its hospitality.

REFERENCES

- Albright B. J., Chandran B. D. G., Cowley S. C., Loh M., 2001, *Phys. Plasmas*, 8, 777
- Bale S. D., Kasper J. C., Howes G. G., Quataert E., Salem C., Sundkvist D., 2009, *Phys. Rev. Lett.*, 103, 211101
- Carilli C. L., Taylor G. B., 2002, *A&A*, 40, 319
- Chandran B. D. G., Cowley S. C., 1998, *Phys. Rev. Lett.*, 80, 3077
- Chandran B. D. G., Cowley S. C., Ivanushkina M., Sydora R., 1999, *ApJ*, 525, 638
- Chandran B. D. G., Maron J. L., 2004, *ApJ*, 602, 170
- Chandrasekhar S., Kaufman A. N., Watson K. M., 1958, *Proc. R. Soc. London A*, 245, 435
- Dennis T. J., Chandran B. D. G., 2005, *ApJ*, 622, 205
- Enßlin T. A., Vogt C., 2006, *A&A*, 453, 447
- Ettori S., Fabian A. C., 2000, *MNRAS*, 317, L57
- Feretti L., Giovannini G., Govoni F., Murgia M., 2012, *A&A Rev.*, 20, 54
- Hasegawa A., 1969, *Phys. Fluids*, 12, 2642
- Hellinger P., Trávníček P., Kasper J. C., Lazarus A. J., 2006, *Geophys. Res. Lett.*, 33, 9101
- Inogamov N. A., Sunyaev R. A., 2003, *Astron. Lett.*, 29, 791
- Kasper J. C., Lazarus A. J., Gary S. P., 2002, *Geophys. Res. Lett.*, 29, 1839
- Klepach E. G., Ptuskin V. S., 1995, *Astron. Letters*, 21, 411
- Komarov S. V., Churazov E. M., Schekochihin A. A., ZuHone J. A., 2014, *MNRAS*, 440, 1153
- Kuchar P., Enßlin T. A., 2011, *A&A*, 529, A13
- Kulsrud R., 1964, in Rosenbluth M. N., ed., *Advanced Plasma Theory General stability theory in plasma physics*. Academic Press, p. 54
- Kunz M. W., Schekochihin A. A., Stone J. M., 2014, *Phys. Rev. Lett.*, 112, 205003
- Kunz M. W., Stone J. M., Bai X.-N., 2014, *J. Comp. Phys.*, 259, 154
- Malyshkin L., 2001, *ApJ*, 554, 561
- Malyshkin L., Kulsrud R., 2001, *ApJ*, 549, 402
- Markevitch M., Mazzotta P., Vikhlinin A., Burke D., Butt Y., David L., Donnelly H., Forman W. R., Harris D., Kim D.-W., Virani S., Vrtilek J., 2003, *ApJ*, 586, L19
- Markevitch M., Ponman T. J., Nulsen P. E. J., Bautz M. W., Burke D. J., David L. P., Davis 2000, *ApJ*, 541, 542
- Markevitch M., Vikhlinin A., 2007, *Phys. Rep.*, 443, 1
- Melville S., Schekochihin A. A., Kunz M. W., 2015, *ArXiv*: 1512.08131

³ And perhaps down by another factor of a few if whistlers are triggered and have the effect predicted by Riquelme et al. (2016).

Narayan R., Medvedev M. V., 2001, ApJ, 562, L129
 Parker E. N., 1958, Phys. Rev., 109, 1874
 Rechester A. B., Rosenbluth M. N., 1978, Phys. Rev. Lett., 40, 38
 Rincon F., Califano F., Schekochihin A. A., Valentini F., 2015, ArXiv: 1512.06455
 Riquelme M., Quataert E., Verscharen D., 2016, ArXiv: 1602.03126
 Ruszkowski M., Begelman M. C., 2002, ApJ, 581, 223
 Schekochihin A., Cowley S., Maron J., Malyskhin L., 2002, Phys. Rev. E, 65, 016305
 Schekochihin A. A., Cowley S. C., 2006, Phys. Plasmas, 13, 056501
 Schekochihin A. A., Cowley S. C., Kulsrud R. M., Hammett G. W., Sharma P., 2005, ApJ, 629, 139
 Schekochihin A. A., Cowley S. C., Taylor S. F., Maron J. L., McWilliams J. C., 2004, ApJ, 612, 276
 Schuecker P., Finoguenov A., Miniati F., Böhringer H., Briel U. G., 2004, A&A, 426, 387
 Skilling J., Mclvor I., Holmes J. A., 1974, MNRAS, 167, 87P
 Spitzer L., 1962, Physics of Fully Ionized Gases. New York: Interscience
 Stone J. M., Gardiner T., 2009, New Astron., 14, 139
 Subramanian K., Shukurov A., Haugen N. E. L., 2006, MNRAS, 366, 1437
 Vikhlinin A., Markevitch M., Murray S. S., 2001, ApJ, 549, L47
 Voigt L. M., Fabian A. C., 2004, MNRAS, 347, 1130
 Zakamska N. L., Narayan R., 2003, ApJ, 582, 162
 Zhuravleva I., Churazov E., Arévalo P., Schekochihin A. A., Allen S. W., Fabian A. C., Forman W. R., Sanders J. S., Simionescu A., Sunyaev R., Vikhlinin A., Werner N., 2015, MNRAS, 450, 4184
 Zhuravleva I., Churazov E., Schekochihin A. A., Allen S. W., Arévalo P., Fabian A. C., Forman W. R., Sanders J. S., Simionescu A., Sunyaev R., Vikhlinin A., Werner N., 2014, Nature, 515, 85

APPENDIX A: TRANSPORT OF A PASSIVE SCALAR

Assume a collisional 1D gas with a linear mean gradient of a scalar quantity a transferred by the gas particles:

$$\langle a(x) \rangle = \text{const} + \alpha x. \quad (\text{A1})$$

Here and below, the angle brackets denote averaging over the particles' distribution. The gradient is sustained by fixed boundary conditions (e.g., walls kept at constant a). The particles can exchange a via collisions. Our goal is to evaluate the flux of a given by

$$q_a = \langle a v_{\parallel} \rangle, \quad (\text{A2})$$

where v_{\parallel} is particle velocity (that is the parallel electron velocity along a field line in application to our problem).

Let us first write the Langevin equation for a particle's velocity:

$$\dot{v}_{\parallel} = -\nu_1 v_{\parallel} + \eta_1(t), \quad (\text{A3})$$

where ν_1 is the particle-scattering collision rate, and $\eta_1(t)$ is a Gaussian white noise with zero mean. Solving for v_{\parallel} gives

$$v_{\parallel} = v_{\parallel}(0)e^{-\nu_1 t} + \int_0^t dt' e^{\nu_1(t'-t)} \eta_1(t'), \quad (\text{A4})$$

and, integrating again,

$$x = x(0) + \frac{v_{\parallel}(0)}{\nu_1}(1 - e^{-\nu_1 t}) + \int_0^t dt' \int_0^{t'} dt'' e^{\nu_1(t''-t')} \eta_1(t''). \quad (\text{A5})$$

The Langevin equation for the evolution of a of a given particle due to collisions reads:

$$\dot{a} = -\nu_2(a - \langle a \rangle) + \eta_2(t), \quad (\text{A6})$$

where ν_2 is the a -exchange collision rate, and η_2 is a Gaussian white noise with zero mean. Solving for a , we get

$$a = a(0)e^{-\nu_2 t} + \nu_2 \int_0^t dt' e^{\nu_2(t'-t)} \langle a[x(t')] \rangle + \int_0^t dt' e^{\nu_2(t'-t)} \eta_2(t'). \quad (\text{A7})$$

Combining equations (A1), (A2) and (A7), we can calculate the scalar flux q_a at time t :

$$q_a = \langle a(t)v_{\parallel}(t) \rangle = \nu_2 \int_0^t dt' e^{\nu_2(t'-t)} \langle \langle a[x(t')] \rangle v_{\parallel}(t) \rangle = \alpha \nu_2 \int_0^t dt' e^{\nu_2(t'-t)} \langle x(t') v_{\parallel}(t) \rangle. \quad (\text{A8})$$

The noise terms do not contribute to the flux because they all have zero mean value. We can express $x(t')$ similar to equation (A5) as

$$x(t') = x(t) - \frac{v_{\parallel}(t)}{\nu_1} [1 - e^{\nu_1(t'-t)}] + \int_t^{t'} dt'' \int_t^{t''} dt''' e^{\nu_1(t'''-t'')} \eta_1(t'''). \quad (\text{A9})$$

Substituting $x(t')$ into equation (A8), we get

$$q_a = -\alpha \langle v_{\parallel}^2(t) \rangle \frac{\nu_2}{\nu_1} \int_0^t dt' e^{\nu_2(t'-t)} [1 - e^{\nu_1(t'-t)}] \rightarrow -\frac{\alpha}{3} \frac{\langle v^2 \rangle}{\nu_1 + \nu_2} \text{ as } t \rightarrow \infty, \quad (\text{A10})$$

where $\langle v_{\parallel}^2(t) \rangle = (1/3)\langle v^2 \rangle$. We see that the flux of the passive scalar a is inversely proportional to the sum of the scattering rate of the particles ν_1 and the a -exchange rate ν_2 . Then the scalar conductivity κ_{a0} is

$$\kappa_{a0} = \frac{1}{3} \frac{\langle v^2 \rangle}{\nu_1 + \nu_2}. \quad (\text{A11})$$

If the particles only exchange a and do not exchange energy, $\langle v^2 \rangle = v^2$.

It is also useful to derive the connection between the scalar flux q_a and the velocity autocorrelation function. Let us first write $x(t')$ as

$$x(t') = x(t) - \int_{t'}^t v_{\parallel}(t'') dt'' \quad (\text{A12})$$

and substitute this into equation (A8):

$$q_a = -\alpha \nu_2 \int_0^t dt' e^{\nu_2(t'-t)} \int_{t'}^t dt'' \langle v_{\parallel}(t'') v_{\parallel}(t) \rangle = -\alpha \nu_2 \int_0^t dt' e^{\nu_2(t'-t)} \int_{t'-t}^0 d\tau \langle v_{\parallel}(t+\tau) v_{\parallel}(t) \rangle$$

$$\rightarrow -\alpha\nu_2 \int_0^\infty dt' e^{-\nu_2 t'} \int_0^{t'} d\tau C(\tau) \text{ as } t \rightarrow \infty, \quad (\text{A13})$$

where $C(\tau) = \langle v_{\parallel}(0)v_{\parallel}(\tau) \rangle$ is the parallel-velocity autocorrelation function. For the conductivity κ_a of the scalar a , we infer

$$\kappa_a = \nu_2 \int_0^\infty dt' e^{-\nu_2 t'} \int_0^{t'} d\tau C(\tau). \quad (\text{A14})$$

With no magnetic mirrors, $C_0(\tau) = (1/3)v^2 e^{-\nu_1 \tau}$, and after substitution of C_0 into equation (A14), we recover equation (A11).

In Section 3.2.3, we demonstrated that in the limit $\lambda/l_B \gg 1$, the parallel velocity autocorrelation function of the monoenergetic electrons in the presence of mirror fluctuations has the form

$$C(t) = \frac{1}{3} S_p v^2 e^{-\nu_{\text{eff}} t}. \quad (\text{A15})$$

The coefficients S_p and ν_{eff} are determined by the Monte Carlo simulations. Now we can express κ_a in terms of these two coefficients and the a -exchange rate ν_2 by substituting $C(t)$ into equation (A14):

$$\kappa_a = \frac{1}{3} \frac{S_p v^2}{\nu_{\text{eff}} + \nu_2} = \frac{1}{3} \frac{S_p v^2}{(\lambda/\lambda_{\text{eff}})\nu_1 + \nu_2}. \quad (\text{A16})$$

By combining equations (A11) and (A16), we obtain the suppression factor of the scalar conductivity κ_a/κ_{a0} :

$$\frac{\kappa_a}{\kappa_{a0}} = S_p \frac{\nu_1 + \nu_2}{(\lambda/\lambda_{\text{eff}})\nu_1 + \nu_2}. \quad (\text{A17})$$

We apply the above formula to relate the suppression of diffusion with the suppression of thermal conduction qualitatively, by taking a to be the electron temperature.